Carbon 257 (2026) 121746

Contents lists available at ScienceDirect

Carbon

journal homepage: www.elsevier.com/locate/carbon

Observation of rainbow scattering in ion transmission through graphene

Carolin Frank [a,b,*], Kevin Vomschee [a], Radek Holeňák [c], Yossarian Liebsch [b], Marika Schleberger [b], Daniel Primetzhofer [a,c]

[a] Materials Physics, Department of Physics and Astronomy, Uppsala University, Regementsvägen 10, Uppsala, 75237, Sweden
[b] Faculty of Physics and CENIDE, University of Duisburg-Essen, Lotharstrasse 1, Duisburg, 47057, Germany
[c] Tandem Laboratory, Uppsala University, Regementsvägen 10, Uppsala, 75237, Sweden

ARTICLE INFO

Keywords:
Rainbow effect
Graphene
Ion-solid interaction
Particle scattering phenomena
Interaction potentials

ABSTRACT

The rainbow effect is a fundamental phenomenon in scattering theory, describing the accumulation of trajectories at characteristic angles associated with Jacobian singularities of the scattering map. In atomically thin materials, rainbow scattering patterns are highly sensitive to projectile-target interactions and lattice symmetry, yet experimental observation has remained elusive. We report the experimental observation of rainbow scattering in ion transmission through single-layer graphene. For 40 keV Xe^+ ions, a circular outer rainbow at 5.28°, associated with maximum binary collision deflection from individual carbon atoms, and a hexagonal inner rainbow at 0.43°, originating from projectiles interacting with multiple carbon atoms, are observed. Molecular dynamics and binary collision simulations reproduce these regimes but fail to capture the measured intensity distribution at the smallest deflection angles when using radially symmetric interaction potentials. These results establish graphene rainbow scattering as an experimental benchmark for interatomic potentials and reveal limitations of common approximations in many-body scattering dynamics.

1. Introduction

The rainbow effect is ubiquitous in various scattering theories of both waves and particles, appearing in contexts ranging from the familiar meteorological phenomenon to nuclear and crystal scattering phenomena. The atomic rainbow effect, first described for semiclassical particle scattering by Ford and Wheeler in 1959, arises when projectiles with different impact parameters are scattered into the same characteristic angle due to Jacobian singularities of the scattering map [1]. Such singularities lead to a caustic (an infinite density of classical trajectories) in angular space, resulting in singularities in the classical differential cross section. Consequently, scattering patterns provide information on the projectile-target interaction potential.

In previous years, rainbow scattering in specular reflection of neutral atoms from surfaces was observed in combination with diffraction patterns, providing insights into projectile-surface interaction [2], [3]. More recent studies of projectile-target interaction focus on diffraction patterns arising from transmission of projectiles through thin films. Discovered by Novoselov and Geim in 2004 [4], graphene is a highly promising material for applications in electronics due to its exceptional electrical, mechanical and thermal properties, and is ideally suited for such transmission experiments due to its monolayer structure and high crystalline quality. Single-layer graphene (SLG) has a hexagonal structure of carbon atoms, corresponding to a single scattering regime in transmission experiments. Diffraction of fast atoms through SLG, just experimentally realized by Kanitz et al. and Guichard et al. revealed diffraction patterns of hydrogen and helium atoms [5], [6], highlighting the unique phenomena accessible in transmission experiments. Diffraction of positronium through graphene has recently provided direct evidence that positronium exhibits wave-like behaviour [7].

Rainbow scattering in graphene provides insights not only into ion-atom interaction potentials, but also into the sample's composition and structure. Several attempts to simulate rainbow scattering in graphene have been made. Recently, simulations for protons transmitted through SLG have been reported [8], [9], [10], [11]. Ćosić et al. suggested rainbow scattering of 5 keV protons in transmission through SLG based on calculations using the ZBL, Molière, and Doyle-Turner potentials [8]. Brand et al. simulated the characteristic rainbow scattering pattern of 5 keV protons transmitted through SLG based on classical trajectories and using the ZBL potential [9]. The simulated results show that graphene's rainbow pattern consists of a hexagonal pattern arising from projectiles with characteristic trajectories interacting with multiple

* Corresponding author. Materials Physics, Department of Physics and Astronomy, Uppsala University, Regementsvägen 10, 75237, Uppsala, Sweden.
E-mail address: carolin.frank@physics.uu.se (C. Frank).

https://doi.org/10.1016/j.carbon.2026.121746
Received 1 May 2026; Received in revised form 28 May 2026; Accepted 5 June 2026
Available online 6 June 2026
0008-6223/© 2026 The Authors. Published by Elsevier Ltd. This is an open access article under the CC BY license (http://creativecommons.org/licenses/by/4.0/).

carbon atoms. However, the experimental observation of rainbow scattering in graphene is challenging due to two essential requirements [11], [12]:

- An unsaturated detector of a very high angular resolution is required to observe a detailed rainbow pattern.
- A single-layer self-supporting graphene of a very high cleanliness is required. Even smallest amounts of contamination – typically introduced in the transfer process – will inevitably enhance multiple scattering of projectiles. Rainbow scattering is sensitive to both orientation and defects of the single-layer graphene as well as to the lattice site of adsorbates. A damaged graphene sheet will result in a blurred scattering pattern due to enhanced multiple scattering.

In this article, we demonstrate the first unambiguous experimental observation of rainbow scattering patterns in ion transmission through single-layer graphene. Based on spatial 2D scattering distributions of scattered projectiles, we show that the rainbow scattering pattern of 40 keV Xe^+ ions transmitted through SLG consists of two parts: A circular outer rainbow and a hexagonal inner rainbow. By combining experiment with simulations based on Molecular Dynamics (MD) for both the Ziegler-Biersack-Littmark (ZBL) [13] and the Nordlund-Lehtola-Hobler (NLH) [14] potential, as well as with simulations based on the Binary Collision Approximation (BCA), we show that the outer rainbow is set by the kinematic limit of close binary collisions between projectiles and individual carbon atoms, whereas the inner rainbow is created by projectiles passing through characteristic regions in a graphene honeycomb experiencing small angle deflection by several carbon atoms simultaneously. The comparison further reveals a key limitation of averaged radially symmetric interaction models in the near-0° regime. Our central result is therefore twofold: the first clear experimental observation of rainbow scattering in transmission through graphene, and a stringent benchmark for modelling interaction between ions and 2D materials in the single-scattering limit.

2. Methods

2.1. Target system

As a target system we used single-layer flattened graphene freely suspended on a transmission electron microscopy (TEM) grid. Graphene on copper was purchased from ACS Material and transferred to a gold TEM grid with a 10-15 nm thick amorphous carbon support foil (Quantifoil R 1.2/1.3 Au grid) following the polymethyl methacrylate (PMMA)-free flattening transfer process described in detail in Ref. [15]. In the target system, regions of self-supporting graphene as well as regions of graphene supported by Quantifoil are present. The degree of coverage is approximately 90%. As discussed below, ions are transmitted exclusively through graphene.

2.2. Transmission experiment

Transmission experiments were performed at the Time-of-Flight Medium Energy Ion Scattering (ToF-MEIS) setup at Uppsala University [16], [17]. A detailed description of sample pretreatment and technical details is included in the Supplementary Information [18].

For the ToF-MEIS measurements, a pulsed beam of singly charged $^{129}Xe^+$ ions with a kinetic energy of 40 keV is transmitted through the target with the monolayer graphene facing the ion beam. Transmitted particles are detected by a circular position-sensitive microchannel plate (MCP, DLD120 from RoentDek [19]), which is positioned 290 mm behind the sample. For this study, the evaluated detector region was limited to a circle with a radius of 40 mm around the position of the direct beam, covering scattering angles of 7.85°. The recorded time-of-flight spectrum for 40 keV $^{129}Xe^+$ ions transmitted through SLG on a gold TEM grid with Quantifoil is shown in Fig. 1, including a schematic of the experiment.

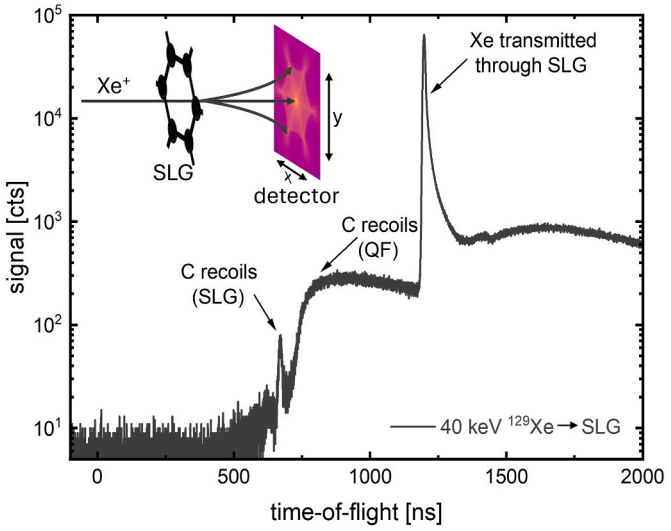

Fig. 1. Time-of-flight spectrum of 40 keV Xe^+ ions transmitted through SLG, including a schematic of the experiment. Dominant peaks are attributed to C recoils from the graphene layer, to C recoils from the Quantifoil and to Xe ions transmitted through SLG.

The peak at 672 ns can be attributed to carbon recoils from the target. A detailed description of elastic recoil detection analysis in transmission time-of-flight ion scattering is given in Ref. [20]. At 40 keV, no Xe ions are transmitted through the Quantifoil. The dominant peak at a flight time of 1198 ns corresponds to Xe ions transmitted through the single-layer graphene, including the direct beam passing through pin holes and damaged areas of the sample. Since virtually no H recoils – expected at 599 ns – are present in Fig. 1, we consider the sample to have a high cleanliness throughout the measurement. To evaluate scattering of Xe ions after transmission through SLG, the spatial distribution of transmitted projectiles on the detector was analyzed for the time-of-flight range corresponding to the dominant graphene peak.

2.3. Simulations

Experimental scattering distributions were compared to scattering distributions simulated using the Molecular Dynamics (MD) Kalypso code [21]. MD simulations explicitly resolve the correlated, time-dependent many-body dynamics. Molecular dynamics simulations were performed using the widely used Ziegler-Biersack-Littmark (ZBL) potential [13] and the recently developed Nordlund-Lehtola-Hobler (NLH) potential, which is based on density functional theory calculations and demonstrated good agreement with experimental results in the energy range from 15 keV to 200 keV [14]:

- ZBL potential: $V(r) = \frac{Z_i Z_j e^2}{4\pi\varepsilon_0 r_{ij}} \sum_{k=1}^{4} c_k e^{\frac{-b_k r_{ij}}{a}}$
- NLH potential: $V(r) = \frac{Z_i Z_j e^2}{4\pi\varepsilon_0 r_{ij}} \sum_{k=1}^{3} c_k e^{-b_k r_{ij}}$

Here, $Z_{i,j}$ denote the atomic numbers of the collision partners, e in the prefactor of the summation is the elementary charge, ε_0 is the dielectric constant, r_{ij} is the distance between collision partners and a is the screening length. For the NLH potential, we used the coefficients b_k and c_k provided in the supplementary material of reference [14] for Xe and C. Note that the b_k parameters have different dimensions in the two potentials.

Simulations were performed at a thermal displacement of 300 K and 500 K for both ZBL and NLH potential to investigate the impact of the thermal displacement on rainbow scattering. Since no differences between MD-simulated scattering distributions for 300 K and 500 K were

observed, we show results for a thermal displacement of 300 K in the present article and include simulation results for 500 K in the Supplementary Information [18]. The employed classical MD framework implemented in Kalypso does not include quantum ground-state motion of the carbon atoms.

Both experimental and MD simulated scattering distributions were compared to simulated ones using the Binary Collision Approximation (BCA) code SIIMPL developed by Janson [22]. In contrast to MD simulations, BCA simulations reduce the interaction potential to independent sequential binary collisions and do not consider collective effects. Here, BCA simulations were performed using the Magic Formula developed by Biersack et al. [13] and assuming the ZBL potential. In the BCA simulations, the carbon atoms were treated classically and include a lattice vibration amplitude of 0.04 Å, as expected at 300 K [23]. Simulation parameters for both MD and BCA simulation are included in the Supplementary Information [18].

3. Results and discussion

Next, we present and discuss the experimental, MD- and BCA-simulated scattering distributions.

3.1. Spatially resolved transmission reveals two rainbows

In Fig. 2a), we present the measured 2D distribution of 40 keV Xe^+ ions transmitted through a self-supporting SLG onto the detector plate. For comparison with Fig. 2a), the MD-simulated 2D distribution of 40 keV Xe^+ ions transmitted through self-supporting SLG is shown in Fig. 2b), using a ZBL potential at random thermal displacements as expected at 300 K. The integrated signal, expressed in counts, is shown color-coded as a function of the scattering angle. According to the charge state distribution shown in Ref. [24], the charge state distribution of transmitted 40 keV Xe projectiles is dominated by neutral Xe atoms.

3.1.1. The outer rainbow is a binary collision limit

Both Fig. 2a) and b) exhibit a distinct and extremely sharp edge, indicated with a dashed line as visual guide in Fig. 2a). This local maximum, referred to as the *outer rainbow* in the following, corresponds to the maximum deflection of Xe projectiles in a binary collision by a single C atom and is thus independent of the projectile's charge state. The observed maximum deflection angle is 5.32°; the classical mechanics limit is 5.34°.

3.1.2. The inner rainbow arises from small angle deflection by multiple carbon atoms

Moreover, both measured and MD-simulated 2D distribution exhibit a hexagonal pattern, referred to as the *inner rainbow* in the following. As visual guide, the shape of the hexagon is indicated with dashed lines in the inset in Fig. 2a). The inner rainbow stems from projectiles with trajectories passing through high-symmetry regions in a graphene honeycomb experiencing small angle deflection by several carbon atoms simultaneously. A reason for the slightly blurred edge of the hexagon might be the presence of small crystal domains in different orientations, as graphene grown via chemical vapour deposition is known to exhibit domains of different orientation. In Fig. 2b), six branches are observed in the distribution between 0° and the angle corresponding to the inner rainbow, which might originate from preferred scattering trajectories through the graphene lattice and are resolved in the classical trajectory picture. In the experiment, these features may not be resolved due to finite angular resolution of the detector and quantum mechanical effects, which lead to a smearing of the fine structure.

For both MD simulation and measurement, the global maximum of the integrated signal is found at the center of the scattering distribution (0°| 0°). In the experimental data, this central position also includes the direct beam transmitted through pinholes in the graphene. However,

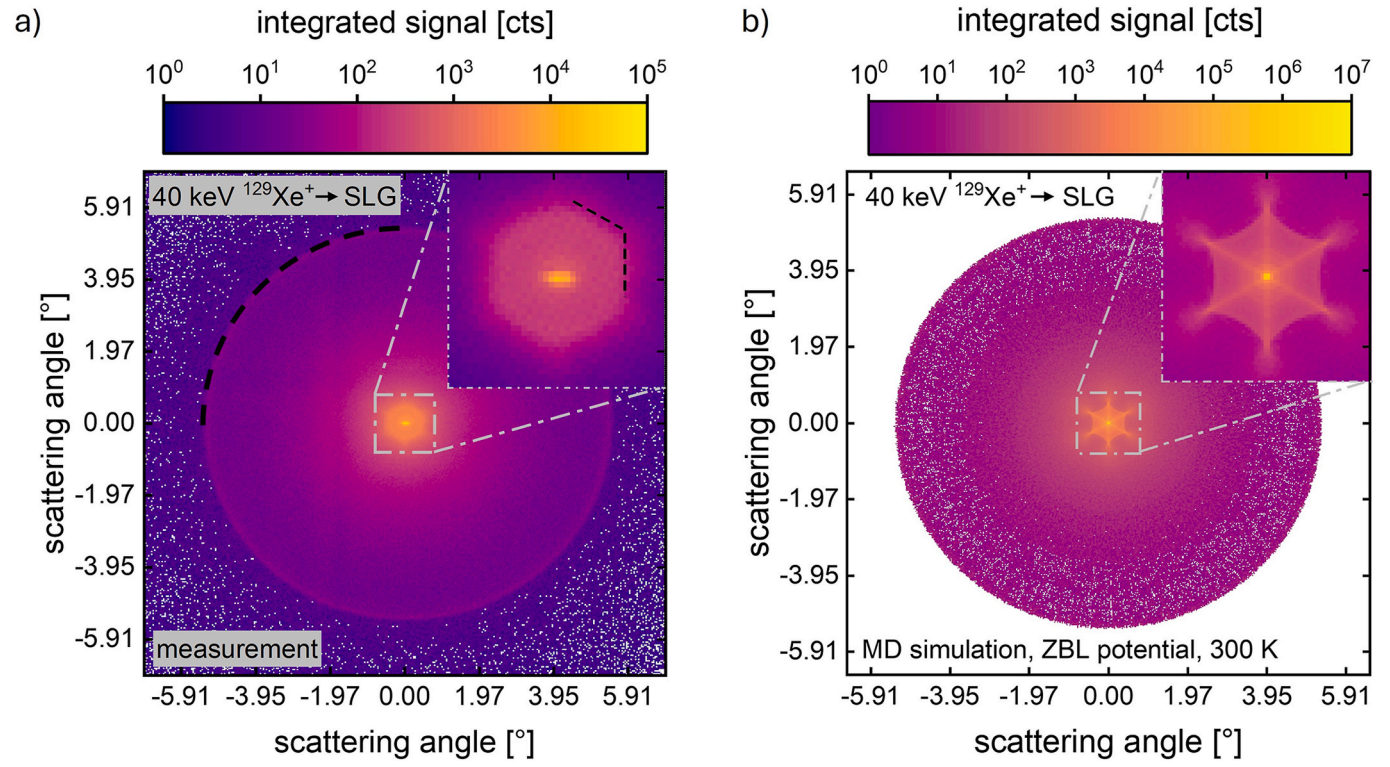

Fig. 2. a) Measured 2D distribution of 40 keV Xe^+ ions transmitted through SLG. As a visual guide, the circular shape of the outer rainbow and the hexagonal shape of the inner rainbow, enlarged in the inset, are indicated with dashed lines. b) MD simulated 2D distribution of 40 keV Xe^+ ions transmitted through SLG using the ZBL potential at a thermal displacement of 300 K. The color scale of the inset in a) and b) is adjusted to enhance the visibility of the features. (For interpretation of the references to color in this figure legend, the reader is referred to the Web version of this article.)

due to the low angular spread of the direct beam, the contribution from pinholes is negligible above 0.16° scattering angle.

3.2. Quantification and comparison of experimental and simulated angular distributions

In Fig. 3, we present the derived angular scattering distributions of 40 keV Xe^+ ions transmitted through self-supporting SLG obtained from a typical measurement (grey), together with angular scattering distributions obtained from MD-simulations using the ZBL potential for 300 K (blue), the NLH potential for 300 K (green), as well as BCA-simulations (purple). For better comparability, the integrated signal height of both measured and BCA-simulated curves is adjusted to the maximum integrated signal of the MD-simulated curves at 5.27°. The uncorrected measurement data as a function of the scattering angle is shown in the Supplementary Information [18]. In the inset of Fig. 3, we show the scattering distributions in the range from 0° to 0.6°.

The angular scattering distributions shown in Fig. 3 differ from each other in terms of scattering angles at which local maxima of the integrated signal occur, the number of maxima, and the shape of the peaks.

In the range from 4.5° to 5.5°, all curves exhibit a peak at similar scattering angles, which corresponds to the outer rainbow (measured: 5.28°, BCA-simulated: 5.25°, MD-simulated: 5.28° for ZBL potential, 5.27° for NLH potential). While all simulated curves show a sharp edge around 5.3°, the edge of the measured peak is smeared out, which is explained predominantly by the divergence of the Xe^+ ion beam. Based on the comparison of measurement and simulations, we conclude that the outer rainbow is independent of the used interaction potential since scattering kinematics is unaffected by conservative potentials.

3.2.1. Potential additional rainbows

In the range from 0.68° to 4.5°, the integrated signal decreases for all curves. In this range, the measured integrated signal is larger than the simulated signals. In comparison to the BCA-simulated curve, the MD-simulated curves show maxima which depend on the used potential (e.g. at 1.08° for ZBL potential and at 1.05° for NLH potential). Around a scattering angle of 2°, a weak feature in the form of locally enhanced intensity is also visible in the measured angular distribution. The respective region is highlighted in Fig. 3 and shown enlarged in the inset

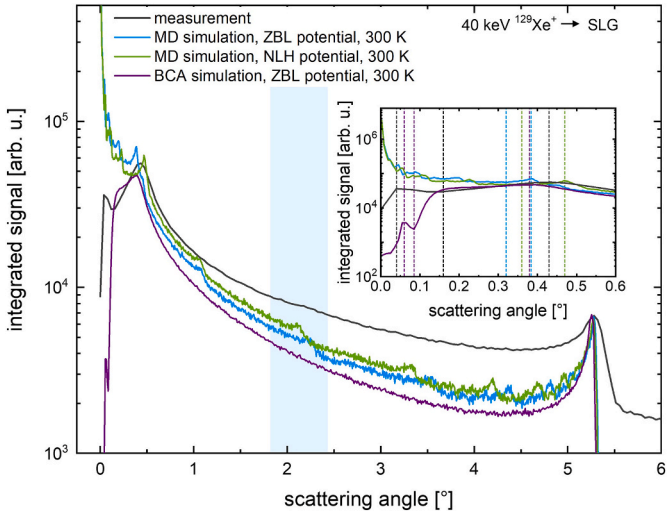

Fig. 3. Integrated signal as a function of the scattering angle as measured (grey), BCA-simulated (purple) and MD-simulated using the ZBL potential (blue) and the NLH potential (green). For better comparability, the integrated signal height of both measured and BCA-simulated curves is adjusted to the maximum integrated signal of the MD-simulated curves at 5.27°. (For interpretation of the references to color in this figure legend, the reader is referred to the Web version of this article.)

of Supplementary Fig. 3. Analysis of standardized residuals revealed local deviations of 3-4 standard deviations for three consecutive data points from the fitted function. We attribute these additional peaks in the MD simulations and in the measurement to *possible additional rainbows,* potentially associated with projectiles experiencing the saddle point in the potential of two carbon atoms in the middle of the honeycomb's edge. However, their identification as rainbow peaks remains conjectural and requires further confirmation in future studies. Alternative origins of the observed features might be interaction with impurities or glory scattering.

Due to the different dependence on the distance r_{ij}, the respective scattering angles differ from each other for ZBL and NLH potential in the MD simulation. Additional rainbows are also visible in the MD-simulated spatial distribution in Fig. 2b) in the form of additional circles with local maxima at scattering angles of 1.19°, 2.36° and 3.66°. In the BCA-simulated angular scattering distribution, no additional peaks are observed because only the potential of a single carbon atom is considered.

3.2.2. Near-0° scattering exposes the limits of radially symmetric interaction potentials

For small scattering angles starting from 0°, both the measured and BCA-simulated scattering distributions rise sharply, reaching a maximum in the integrated signal (measurement: 0.04°, BCA simulation: 0.06°), followed by a local minimum (measurement: 0.16°, BCA simulation: 0.08°). In contrast to that, the MD-simulated integrated signal decreases from a maximum at 0°, reaching a minimum at 0.32° for the ZBL potential and at 0.36° for the NLH potential. All curves show a dominant peak in the range from 0.3° to 0.5°, corresponding to the inner rainbow. In the measurement, the inner rainbow is found at a scattering angle of 0.43°, while in the BCA simulation it shifted to 0.35°. In contrast to the outer rainbow, the inner rainbow depends on the applied interaction potential (ZBL: 0.38°, NLH: 0.47°) due to the different dependence of the respective potential on the distance between projectile and C atom. In the BCA simulation, the inner rainbow arises because the set of impact parameters is limited to the hexagonal Wigner-Seitz cell of the graphene crystal. Hence, in the BCA simulation, the integrated signal decreases towards zero at a scattering angle of 0°. In the MD simulations, these effects are supplemented by the superposition of the potentials of the surrounding carbon atoms. Due to the superposition of the potentials and the resulting rather flattened potential landscape between neighboring carbon atoms, the MD simulations show a strong increase towards a maximum value of the integrated signal around a scattering angle of 0°.

Radially symmetric potentials exhibit several symmetry points when superimposed onto each other in graphene, resulting in 0° deflection being likely, as observed in the MD simulations. These symmetry points associated with 0° scattering scenarios – such as central impact on a C atom, passage through the center of a hexagon, or through the midpoint between two C atoms – are illustrated schematically in the Supplementary Information [18]. However, the measured angular distribution shows a decreasing signal towards 0°, indicating that 0° scattering is rare despite being geometrically possible. This observation can, on the one hand, be attributed to the actual potential being non-radially symmetric – e.g., due to chemical bonds – in particular at comparably large interaction distances relevant for deflections near 0°. On the other hand, the scattering regime near 0° is highly sensitive to electronic processes: charge exchange between Xe and SLG alters the effective interaction potential along the projectile's trajectory [24], [25], [26], which thus varies for each projectile and is particularly important for two-dimensional target systems in the single scattering regime. Accounting for associated momentum transfers to the electrons, leading to small angle deflections, further reduces the probability of 0° scattering. We therefore conclude that averaged, radially symmetric potentials, as assumed in the MD simulations, are insufficient to accurately describe the here investigated projectile-target interaction.

4. Conclusion

We have observed the rainbow scattering pattern of 40 keV Xe^+ ions transmitted through self-supporting single-layer graphene. The measured rainbow pattern contains two distinct components with different origins: an outer circular rainbow solely determined by kinematics, and a hexagonal inner rainbow arising from projectiles passing through characteristic regions in a graphene honeycomb experiencing small angle deflection by several carbon atoms. This establishes a direct experimental signature of rainbow scattering in particle transmission through graphene.

Comparison with molecular dynamics and binary collision approximation simulations shows a clear disparity in the capabilities of current models. The outer rainbow is reproduced by scattering kinematics and is largely insensitive to the choice of interaction potential. By contrast, the measured distribution at the smallest deflection angles, particularly in the near-0° regime, is not captured by averaged radially symmetric potentials.

With this study, we open the door to investigate interatomic potentials and their dynamics in solids in unprecedented detail via transmission experiments. Our work can easily be extended to include more complex interaction scenarios such as experiments with multiply charged ions, molecular beams or 2D materials beyond graphene, e.g. transition metal dichalcogenides. These opportunities will provide insights into electronic structures and screening effects specific to 2D materials – and exceptional access to semiclassical dynamics.

CRediT authorship contribution statement

Carolin Frank: Conceptualization, Data curation, Formal analysis, Investigation, Methodology, Software, Visualization, Writing – original draft. **Kevin Vomschee:** Conceptualization, Investigation, Methodology, Software, Writing – review & editing. **Radek Holeňák:** Investigation, Software, Writing – review & editing. **Yossarian Liebsch:** Investigation. **Marika Schleberger:** Conceptualization, Funding acquisition, Project administration, Resources, Supervision, Writing – review & editing. **Daniel Primetzhofer:** Conceptualization, Funding acquisition, Project administration, Resources, Supervision, Writing – review & editing.

Declaration of competing interest

The authors declare that they have no known competing financial interests or personal relationships that could have appeared to influence the work reported in this paper.

Acknowledgements

Accelerator operation is supported by the Swedish Research Council VR-RFI (Contract No. 2023-00155). C. F. and M. S. acknowledge financial support from the DFG (CRC 1242 “Non-Equilibrium Dynamics of Condensed Matter in the Time Domain”, project number 278162697, and “2D Mature”, project number 461605777) and from the Faculty of Physics.

Appendix A. Supplementary data

Supplementary data to this article can be found online at https://doi.org/10.1016/j.carbon.2026.121746.

Data availability

Data is available under https://doi.org/10.5281/zenodo.19000681.

References

[1] K.W. Ford, J.A. Wheeler, Semiclassical description of scattering, Ann. Phys. 7 (1959) 259–286, https://doi.org/10.1016/0003-4916(59)90026-0.
[2] A. Schüller, S. Wethekam, H. Winter, Diffraction of fast atomic projectiles during grazing scattering from a LiF(001) surface, Phys. Rev. Lett. 98 (2007), https://doi.org/10.1103/PhysRevLett.98.016103.
[3] P. Rousseau, H. Khemliche, A.G. Borisov, P. Roncin, Quantum scattering of fast atoms and molecules on surfaces, Phys. Rev. Lett. 98 (2007), https://doi.org/10.1103/PhysRevLett.98.016104.
[4] K.S. Novoselov, et al., Electric field effect in atomically thin carbon films, Science 306 (2004) 666–669, https://doi.org/10.1126/science.1102896.
[5] C. Kanitz, et al., Diffraction of helium and hydrogen atoms through single-layer graphene coherent diffraction in transmission, Science 389 (2025) 724–726, https://doi.org/10.1126/science.adx5679.
[6] P. Guichard, et al., Fast hydrogen atom diffraction through monocrystalline graphene, Phys. Rev. Lett. 135 (2025), https://doi.org/10.1103/wdx6-mrvm.
[7] Y. Nagata, et al., Observation of positronium diffraction, Nat. Commun. 17 (2026), https://doi.org/10.1038/s41467-025-67920-0.
[8] M. Ćosić, S. Petrović, N. Nešković, The forward rainbow scattering of low energy protons by a graphene sheet, Nucl. Instrum. Methods Phys. Res. B 422 (2018) 54–62, https://doi.org/10.1016/j.nimb.2018.02.028.
[9] J. Bühler, P. Roncin, C. Brand, Describing the scattering of keV protons through graphene, Front. Chem. 11 (2023), https://doi.org/10.3389/fchem.2023.1291065.
[10] C. Brand, et al., Coherent diffraction of hydrogen through the 246 pm lattice of graphene, New J. Phys. 21 (2019), https://doi.org/10.1088/1367-2630/ab05ed.
[11] M. Ćosić, et al., Morphological study of the rainbow scattering of protons by graphene, Chaos 31 (2021), https://doi.org/10.1063/5.0059093.
[12] N. Watanabe, et al., Rainbow scattering pattern of fast ions by graphene sheet, Nucl. Instrum. Methods Phys. Res. B 553 (2024), https://doi.org/10.1016/j.nimb.2024.165380.
[13] J.F. Ziegler, J.P. Biersack, U. Littmark, The Stopping and Range of Ions in Solids, Pergamon, 1985.
[14] K. Nordlund, S. Lehtola, G. Hobler, Repulsive interatomic potentials calculated at three levels of theory, Phys. Rev. A 111 (2025), https://doi.org/10.1103/PhysRevA.111.032818.
[15] L. Madauß, et al., A swift technique to hydrophobize graphene and increase its mechanical stability and charge carrier density, npj 2D Mater. Appl. 4 (2020), https://doi.org/10.1038/s41699-020-0148-9.
[16] M.A. Sortica, et al., A versatile time-of-flight medium-energy ion scattering setup using multiple delay-line detector, Nucl. Instrum. Methods Phys. Res. B 463 (2020) 16–20, https://doi.org/10.1016/j.nimb.2019.11.019.
[17] M.K. Linnarsson, et al., New beam line for time-of-flight medium energy ion scattering with large area position sensitive detector, Rev. Sci. Instrum. 83 (2012), https://doi.org/10.1063/1.4750195.
[18] See supplementary information for sample preparation, Technical Details, Simulation Parameters and Additional Data.
[19] O. Jagutzki, et al., A broad-application microchannel-plate detector system for advanced particle or photon detection tasks: large area imaging, precise multi-hit timing information and high detection rate, Nucl. Instrum. Methods Phys. Res. 477 (2002) 244–249, https://doi.org/10.1016/S0168-9002(01)01839-3.
[20] R. Holeňák, et al., Sensitive multi-element profiling with depth resolution enabled by time-of-flight recoil detection in transmission using pulsed keV ion beams, Vacuum 204 (2022), https://doi.org/10.1016/j.vacuum.2022.111343.
[21] M.A. Karolewski, Kalypso: a software package for molecular dynamics simulation of atomic collisions at surfaces, Nucl. Instrum. Methods Phys. Res. B 230 (2005) 402–405, https://doi.org/10.1016/j.nimb.2004.12.074.
[22] M. Janson, Hydrogen Diffusion and Ion Implantation in Silicon Carbide, PhD thesis, 2003.
[23] C.S. Allen, et al., Temperature dependence of atomic vibrations in mono-layer graphene, J. Appl. Phys. 118 (2015), https://doi.org/10.1063/1.4928324.
[24] R. Holeňák, et al., Charge state distributions of Xenon ions with keV kinetic energies transmitted through graphene and carbon self-supporting foils, Nucl. Instrum. Methods Phys. Res. B 554 (2024), https://doi.org/10.1016/j.nimb.2024.165415.
[25] A. Niggas, et al., Charge exchange of slow highly charged ions from an electron beam ion trap with surfaces and 2D materials, J. Phys. B 57 (2024), https://doi.org/10.1088/1361-6455/ad2e2a.
[26] R.A. Wilhelm, P. Grande, Unraveling energy loss processes of low energy heavy ions in 2D materials, Commun. Phys. 2 (2019), https://doi.org/10.1038/s42005-019-0188-7.